A Predictor of Turbulent Kinetic Energy for Oscillatory Flows Through Submerged Aquatic Vegetation

Jorge E. San Juan[1,2], and Rafael O. Tinoco[2]

[1]St. Anthony Falls Laboratory, Department of Civil, Environmental, and Geo-Engineering, University of Minnesota Twin Cities, MN, USA
[2]Ecohydraulics and Ecomorphodynamics Laboratory, Department of Civil and Environmental Engineering, University of Illinois Urbana-Champaign, IL, USA

Key Points:

- Models for unidirectional vegetated flows can be adapted to estimate turbulence metrics in oscillatory flows.
- Maximum turbulent kinetic energy at the top of the submerged canopies is a function of vegetation density and wave orbital velocity.
- Maximum near-bed turbulent kinetic energy is a function of depth-averaged velocities and vegetation density.

Corresponding author: Jorge E. San Juan, jsanjuan@umn.edu

Abstract

Aquatic vegetation modifies hydrodynamics, turbulence structure, sediment transport, and ecological processes in marine ecosystems. Recent turbulence models for vegetated flows have focused on open channel unidirectional flows. However, the unsteadiness and turbulent structure of oscillatory flows often prevent the direct application of such models in wave-dominated environments. We investigate Turbulent Kinetic Energy (TKE) connected to the flow structure in oscillatory flows through aquatic vegetation. Using an oscillatory tunnel, we test vegetation densities up to $\phi = 0.10$ with wave periods between 2.1-5.3 s and wave amplitudes between 2-10 cm. Our measurements show a nonlinear relation between the TKE inside the canopy and vegetation density due to the change from the stem- to canopy-scale dominated regime. We observe that $ah \geq 0.8$ marks a threshold for this transition: a reduction of wake TKE inside the canopy and an increase of shear TKE at the top of the canopy. This transition is characterized by increasing frequency and intensity of sweeps and ejections near the bed and at the canopy top. We developed a two-equation predictor for TKE at the top of the canopy using the "short-cut" TKE transfer first proposed by Finnigan (2000) where canopy-scale eddies convert TKE into stem-scale eddies via the work against vegetation drag. For near-bed TKE, we adapt Tanino and Nepf (2008b)'s model to predict the maximum TKE values on oscillatory flows. These two predictors provide easy-to-use tools suitable for wave-dominated environments to accurately estimate TKE levels inside the canopy for estimating sediment transport rates and mass exchange across the canopy.

Plain Language Summary

Plants change water movement, turbulence, sediment routing, and ecological processes in aquatic ecosystems. Recent turbulence models for vegetated flows have focused on open-channel conditions. However, time-dependency and turbulent structure in waves often prevent the direct application of such models in marine environments. Inaccurate estimations of turbulence levels lead to erroneous calculations of sediment and mass transport in aquatic ecosystems. We investigate the turbulent kinetic energy (TKE) in waves through submerged vegetation in a laboratory. We propose two predictors for the maximum TKE at two critical locations: near the bed and at the vegetation top. Our measurements show a nonlinear relation between the TKE inside the plants and vegetation density due to the transition between stem- to canopy-flow structures. We observe a reduction of stem-TKE inside the meadow and an increase of shear-TKE at the top of the plants at a certain vegetation density threshold. We developed a two-equation predictor for TKE at the top of the vegetation using the "short-cut" TKE transfer mechanism. For near-bed TKE, we adapt an open-channel flow model to predict the maximum TKE values. These two predictors provide easy-to-use tools suitable for wave-dominated environments to estimate TKE levels inside the canopy accurately.

1 Introduction

Morphological changes in shallow marine ecosystems result from the long-term nonlinear summation of small scale processes (Perillo & Piccolo, 2011). Such processes often depend on aquatic vegetation, which interacts with the flow to alter hydrodynamics, turbulence structure, sediment transport, and ecological processes (Leonard & Luther, 1995; Bouma et al., 2007; Norris et al., 2017; Davis et al., 2020). Numerous studies have focused on vegetation-generated turbulence on open channel flows (e.g., López & García, 2001; Ghisalberti & Nepf, 2002; Tanino & Nepf, 2008b), and predictors from those studies have been used in wave-dominated environments (e.g., Y. Zhang et al., 2018; Chen et al., 2020; Tseng & Tinoco, 2021). However, hydrodynamics and turbulence structure between these two environments differ greatly. The unsteadiness and reversible nature of oscillatory flows create out-of-phase internal structures between the inside- and above-

vegetation regions (Pujol, Casamitjana, et al., 2013; Pujol, Serra, et al., 2013). These characteristics impact the turbulence generation at ecologically important regions of the flow (Abdolahpour et al., 2018), such as the canopy top, the in-canopy wake region, and near the bed, compromising the direct application of unidirectional flow models in oscillatory environments.

Inaccurate estimation of vegetation-induced turbulence may lead to poor predictions of sediment transport. Studies have found that Turbulent Kinetic Energy (TKE) is the main driver for sediment motion in canopy flows (e.g., Tinoco & Coco, 2018; Yang & Nepf, 2018; J. Zhang et al., 2020; Shan et al., 2020; Tseng & Tinoco, 2021). Lowe, Koseff, and Monismith (2005) observed that in-canopy velocity in oscillatory flows are not damped as significantly as in unidirectional flows, which results in increased turbulence intensities compared with similar array densities and undisturbed velocities. Chen et al. (2020) found different contributions from shear-induced canopy-scale turbulence in the TKE vertical distribution under pure waves and unidirectional currents. Their findings suggest that the implementation of unidirectional turbulence predictors needs to be adjusted for an appropriate application in wave-dominated environments. Underestimating turbulence levels, which serve as a proxy for sediment transport in aquatic ecosystems, may impact conservation and restoration practices that seek to promote bed aggradation, alter residence time, and encourage biodiversity through vegetation.

The mechanisms that generate turbulence in vegetated flows (such as bed shear, stem-wake, and top canopy shear) change spatially and temporally in oscillatory flows (Nepf, 2012). Due to the unsteady nature of oscillatory flows, previous work studied the nonlinear association between turbulence production and vegetation-flow interactions (e.g., Hansen & Reidenbach, 2017; Abdolahpour et al., 2018; Norris et al., 2019; Chen et al., 2020). They pointed out the competing mechanisms of wave dissipation and stem-turbulence production as the reason for turbulence variations inside the canopy as a function of vegetation density. Y. Zhang et al. (2018) developed a model for TKE in the stem region for oscillatory flows based on the model of Tanino and Nepf (2008b). Y. Zhang and Nepf (2019) studied the connection with sediment resuspension and the near-bed turbulence processes. Tang et al. (2019) validated Y. Zhang et al. (2018)'s TKE predictor and assessed the critical velocity for sediment resuspension. However, their models rely on mean values of TKE, whereas sediment pick up mechanisms can be more related to high bursts of turbulent events (Yang & Nepf, 2018). Chen et al. (2020) found a TKE predictor as a function of canopy elevation observing a correlation between vegetation density and turbulence. Similarly to previous studies, they assume that wake production equals dissipation and it takes place at a constant rate. Nevertheless, at the top of the canopy there is TKE transfer from canopy-scale eddies into wake turbulence as a function of vegetation drag (Finnigan, 2000; King et al., 2012; Zhao et al., 2020). Such ecologically important, shear-driven instabilities at the top of the canopy are responsible for the mass exchange across the top of the canopy (Lowe, Koseff, Monismith, & Falter, 2005; Wong et al., 2019).

We investigate the TKE at the top of the canopy and near the bed associated with the flow structure in oscillatory flows through submerged rigid vegetation. We propose two predictors for the maximum TKE at two critical locations for sediment transport and mixing within vegetation: the canopy-top and the near-bed region, as a function of vegetation density and characteristic velocity. The top-of-the-canopy TKE predictor is based on the TKE transfer from canopy- to stem-scale turbulence in the mixing layer. The near-bed TKE predictor uses Tanino and Nepf (2008b) model's structure but allows for a vegetation density-dependence of the rate of turbulence dissipation.

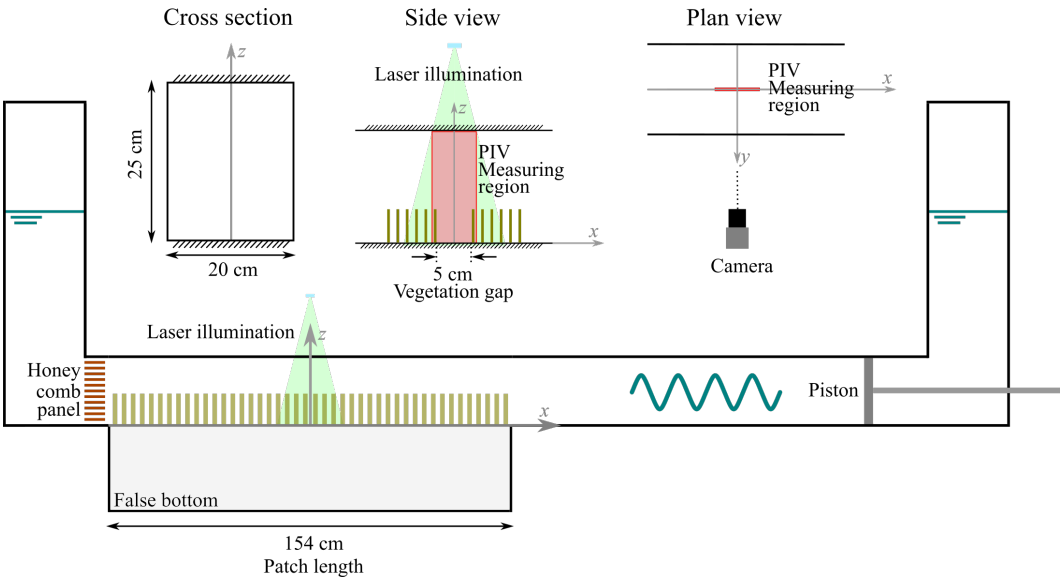

Figure 1. Illustration of experimental setup showing an overview of the oscillatory tunnel, rectangular cross section, and details of the measuring region.

2 Methodology

We use a U-shaped oscillatory tunnel with smooth transparent acrylic walls, 20 cm-wide by 25 cm-height cross section, and 154 cm-long test section. Controlled through a National Instruments Card and LabView script, a piston-actuator system produces sinusoidal oscillatory flows with a maximum 10 cm stroke and minimum 2 s period. A 15 cm-long honeycomb structure seats at the piston-opposite end of the tunnel to straighten the incoming flow from the tunnel's chimney (see fig. 1).

Randomly distributed arrays of acrylic cylinders, 0.63 cm-diameter and 8 cm-height, stand on a mobile bed composed of crushed walnut shells ($\rho = 1.2$ g cm^{-3} and $D_{50} =$ 1 mm) to simulate patches of submerged rigid vegetation. We designed the arrays to ensure symmetry along the x (at the center of the array) and y axis (at the centerline of the tunnel) to prevent the emergence of preferential flow patterns. Table 1 presents a summary of the six vegetation conditions used in this study along with their vegetation parameters. Equations 1 to 4 define the mean stem separation $\langle s_n \rangle_A$ (mean surface-to-surface separation between cylinders), number of stems per unit of area m, volumetric frontal area a (total frontal area per unit of control volume), and volumetric solid fraction ϕ (volume of vegetation per unit of control volume). Here, N_{stem} is the total number of stems in the patch, $s_{\min}$ is the minimum surface-to-surface stem separation, L_x is patch length, L_y is patch width, and d is stem diameter.

$$\langle s_n \rangle_A = \frac{1}{N} \sum_{n=1}^{N_{\text{stem}}} s_{\min,n} \tag{1}$$

$$m = \frac{N}{L_x L_y} \approx \frac{1}{\langle s_n \rangle_A^2} \tag{2}$$

$$a = \frac{Nd}{L_x L_y} \approx \frac{d}{\langle s_n \rangle_A^2} = dm \tag{3}$$

$$\phi = \frac{N(\pi d^2/4)}{L_x L_y} \approx \frac{\pi d^2/4}{\langle s_n \rangle_A^2} = \frac{\pi d^2 m}{4} \tag{4}$$

Three flow conditions are imposed, with oscillation periods T between 2.1 to 5.3 s and piston strokes A between 2 to 10 cm. Table 1 summarizes all experimental cases. Based on Keulegan-Carpenter number (KC=$U_\infty T/d$, with U_∞ being maximum outer flow velocity), flow conditions in combination with vegetation density lie within a regime characterized by vortex shedding at the top of the canopy, and wake generation inside the canopy, with weak inertia effect (Ghisalberti & Schlosser, 2013). Wave Reynolds number (Re= $U_\infty A/\nu$, where ν is kinematic viscosity) between $1,031 - 18,716$, and stem-diameter Reynolds number ($\mathrm{Re}_d = U_\infty A/\nu$) between 287−925, as presented in table 1.

Two-component two-dimensional (2C-2D) velocity fields are measured inside a 5 cm gap within the vegetation patch using particle image velocimetry (PIV). A 5W, 532nm continuous wave laser was used as light source. We used a 5-Megapixel CCD Camera (JAI GO-5000M-USB3) to capture instantaneous velocity fields in a 5 cm long by 25 cm high region that covers the whole tunnel height. The captured images yield a spatial resolution of 74 px cm^{-1}. As function of maximum outer velocity U_∞, we acquire images between $33 - 111$ frames-per-second (fps), yielding Δt values between $9 - 30$ ms. Images were processed using PIVLab (Thielicke & Stamhuis, 2014) using two passes with subwindow interrogation areas from 64×64 to 32×32 pixels, yielding velocity fields with a 2 mm spatial resolution.

Instantaneous velocity components u and w correspond to the longitudinal, x and vertical z directions, respectively. We decompose velocity measurements according to equation 5; where $\overline{u}$ is time-averaged velocity, $\widetilde{u}$ is phase-averaged velocity (see eq. 6), and u' is turbulent velocity fluctuation. $\omega = 2\pi/T$ is angular velocity; N_{osc} is the total number of waves measured (Jensen et al., 1989). Spatial averaging is denoted by the operator $\langle\rangle_{i,k}$ where subscripts indicate the axis along which averaging is conducted. Equations 7 and 8 show the spatial averaging of a longitudinal velocity 2D field into a z-profile, and single point, respectively. N_x, N_z are total number of velocity points along coordinates x, and z, respectively. We analyze temporal and spatial turbulence characteristics through phase-averages of the turbulent kinetic energy $\widetilde{k}$. TKE is defined in equation 9, where u' and w' are turbulent velocity fluctuations from the wave decomposition (see eq. 5).

$$u(x, z, \omega t) = \overline{u}\,(x, z) + \widetilde{u}\,(x, z, \mathrm{mod}\,(t, T)\,\omega) + u'\,(x, z, \omega t) \tag{5}$$

$$\widetilde{u}\,(x, z, \mathrm{mod}\,(t, T)\,\omega) = \frac{1}{N_{\mathrm{osc}}} \sum_{n=1}^{N_{\mathrm{osc}}} [u(x, z, (t + nT)\omega) - \overline{u}] \tag{6}$$

$$\langle u \rangle_x = \frac{1}{N_x} \sum_{i=1}^{N_x} u(x_i, z_k, \omega t) \tag{7}$$

$$\langle u \rangle_{xz} = \frac{1}{N_x N_z} \sum_{i=1}^{N_x} \sum_{k=1}^{N_z} u(x_i, z_k, \omega t); \tag{8}$$

$$\widetilde{k}(x, z, \omega t) = \frac{1}{2} \left(2\widetilde{u'^2} + \widetilde{w'^2} \right) \tag{9}$$

Table 1. Summary of all experimental cases. Wave Reynolds number Re= $U_\infty A/\nu$, where ν is kinematic viscosity. Stem-diameter Reynolds number $\mathrm{Re}_d = U_\infty A/\nu$. Keulegan-Carpenter number KC=$U_\infty T/d$, with U_∞ being maximum outer flow velocity.

N	m [m^{-2}]	a [cm^{-1}]	ϕ [1]	s [cm]	T [s]	A [cm]	U_∞ [cm s^{-1}]	U_{in} [cm s^{-1}]	Re [1]	$\mathrm{Re_d}$ [1]	KC [1]
928	3114	0.20	0.10	1.79	2.1	2	5.3	4.5	1052	287	15
					2.1	3	7.9	6.8	2359	434	23
					2.1	5	12.8	10.5	6419	667	35
					2.1	6	15.4	11.5	9225	732	39
					3.2	3	5.4	4.7	1634	298	24
					3.2	5	9.0	7.4	4506	468	37
					3.2	7	12.9	9.2	9031	585	46
					3.2	10	18.7	12.8	18716	810	64
					5.3	7	7.9	6.0	5508	381	50
					5.3	9	10.4	7.5	9323	479	63
					5.3	10	11.7	8.1	11675	515	68
696	2336	0.15	0.07	2.07	2.1	2	5.3	4.9	1055	310	16
					2.1	3	7.8	7.4	2335	472	25
					2.1	5	12.7	11.4	6348	723	38
					2.1	6	15.1	12.3	9067	781	41
					3.2	3	5.3	5.2	1596	332	26
					3.2	5	8.8	8.0	4392	505	40
					3.2	7	12.5	10.3	8726	653	52
					3.2	10	18.1	13.6	18095	865	69
					5.3	7	7.6	6.4	5355	409	54
					5.3	9	10.1	8.1	9046	513	68
					5.3	10	11.3	8.6	11336	547	72
464	1557	0.10	0.05	2.53	2.1	2	5.5	4.9	1094	311	16
					2.1	3	8.0	7.3	2407	461	24
					2.1	5	13.1	11.1	6570	705	37
					2.1	6	15.9	12.4	9511	789	42
					3.2	3	5.5	5.1	1652	321	25
					3.2	5	9.0	7.9	4519	501	40
					3.2	7	12.8	10.1	8961	638	51
					3.2	10	18.6	13.9	18608	883	70
					5.3	7	7.8	6.5	5484	415	55
					5.3	9	10.3	8.0	9227	505	67
					5.3	10	11.5	8.5	11467	542	72
348	1168	0.07	0.04	2.93	2.1	2	5.4	5.4	1086	343	18
					2.1	3	8.1	7.9	2437	503	27
					2.1	5	13.2	12.3	6589	780	41
					2.1	6	15.8	14.6	9502	925	49
					3.2	3	5.5	5.4	1657	341	27
					3.2	5	9.0	8.6	4500	546	43
					3.2	7	12.7	10.8	8865	689	55
					3.2	10	18.0	14.3	18005	911	72
					5.3	7	7.8	7.1	5426	450	59
					5.3	9	10.1	8.5	9061	541	72
					5.3	10	11.2	8.9	11225	568	75
232	779	0.05	0.02	3.58	2.1	2	5.2	5.1	1031	322	17
					2.1	3	7.6	7.5	2286	475	25
					2.1	5	12.3	12.0	6167	760	40
					2.1	6	14.7	13.8	8840	878	46
					3.2	3	5.2	5.1	1551	325	26
					3.2	5	8.5	8.4	4250	535	42
					3.2	7	11.9	10.7	8347	682	54
					3.2	10	16.9	13.4	16864	853	68
					5.3	7	7.2	6.7	5066	427	56
					5.3	9	9.4	8.3	8476	529	70
					5.3	10	10.5	8.2	10499	523	69

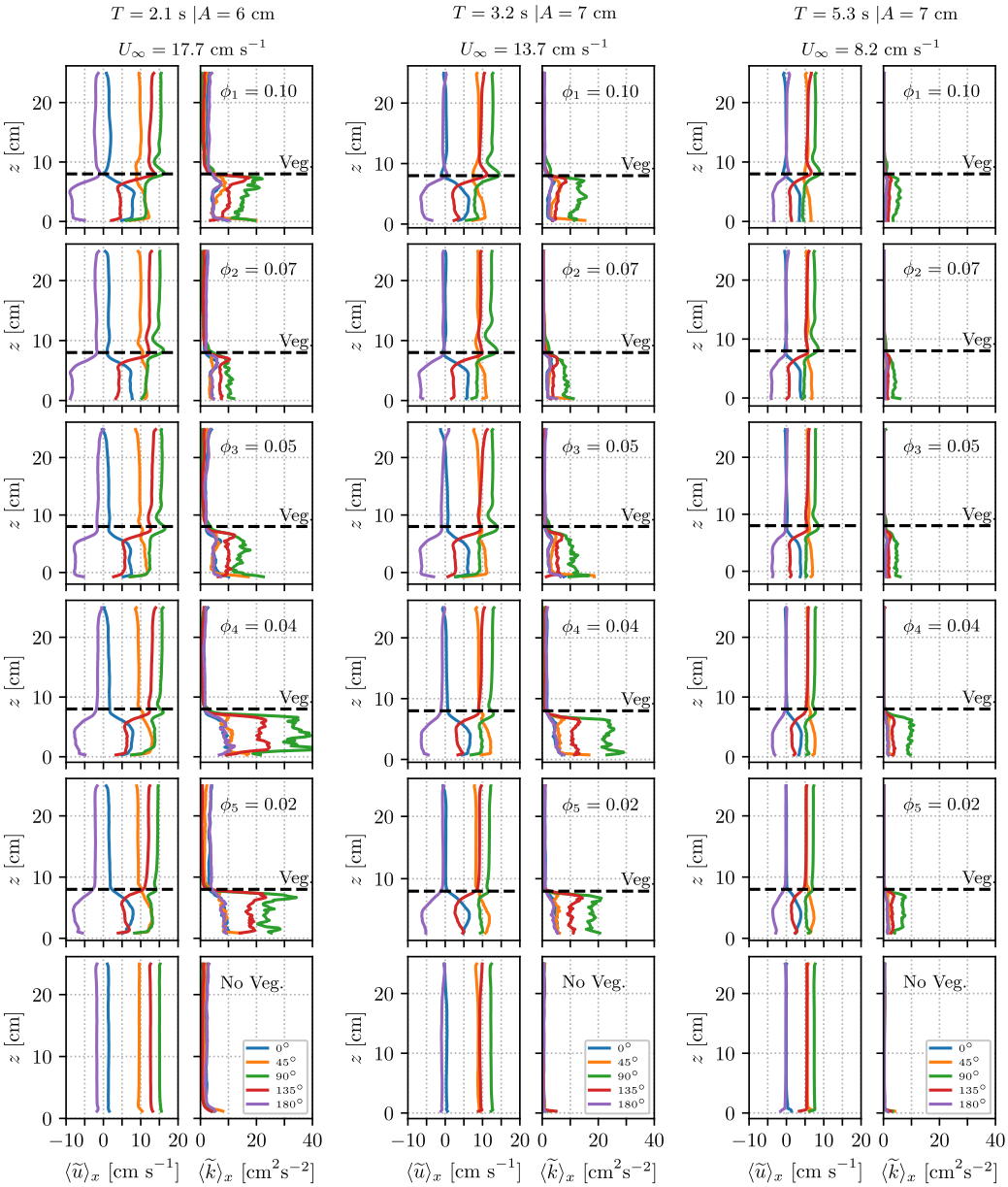

Figure 2. Phase-averaged longitudinal velocity and TKE profiles over the half positive-velocity cycle for flow conditions [$T = 2.1$ s and $A = 6$ cm], [$T = 3.2$ s and $A = 7$ cm], and [$T = 5.3$ s and $A = 7$ cm] across six vegetation conditions from $\phi_1 = 0.10$ to ϕ_0 (no-vegetation).

3 Results

3.1 Velocity and Turbulent Kinetic Energy

Vegetation density, wave amplitude, and wave period drive changes in flow structures in vegetated oscillatory flows. Figure 2 shows the phase-averaged longitudinal velocity and TKE profiles over the half positive-velocity cycle (0° to 180°). It presents three flow conditions across six vegetation conditions. Two different regions are clearly noticed: above-canopy and inside-canopy, with $z/h > 1$ and $z/h \leq 1$, respectively (where h is vegetation height). Velocity inside the canopy is slower than the outer flow above the canopy, while turbulence is higher in the canopy region than above the vegetation. In consequence, the inertia difference between these two regions influences their response time during acceleration and deceleration phases.

Maximum values of turbulent kinetic energy inside the canopy follow a non-monotonic relation with vegetation density. For instance, take the variation of the TKE profile at 90° from the non-vegetated case to the highest vegetation density $\phi_1 = 0.1$ in figure 2. Increasing vegetation density from $\phi_5 = 0.02$ to $\phi_4 = 0.04$ increases TKE. However, the transition between $\phi_4 = 0.04$ to $\phi_3 = 0.05$ reduces the turbulence levels inside the canopy. This decrease continues as the vegetation density increases from $\phi_3 = 0.05$ to $\phi_2 = 0.07$. Nonetheless, as density increases to $\phi_1 = 0.1$, TKE recovers to magnitudes comparable to the $\phi_3 = 0.05$ condition. While previous studies found turbulence increasing with increasing density, we notice that while the stem-wake contribution might increase, the canopy-scale contribution in the presence of shear layer eddies can impact the vertical distribution of TKE. Thus, canopy-scale eddies affect TKE profiles, depending on whether they are arrested at the top of the canopy or can penetrate deep within it.

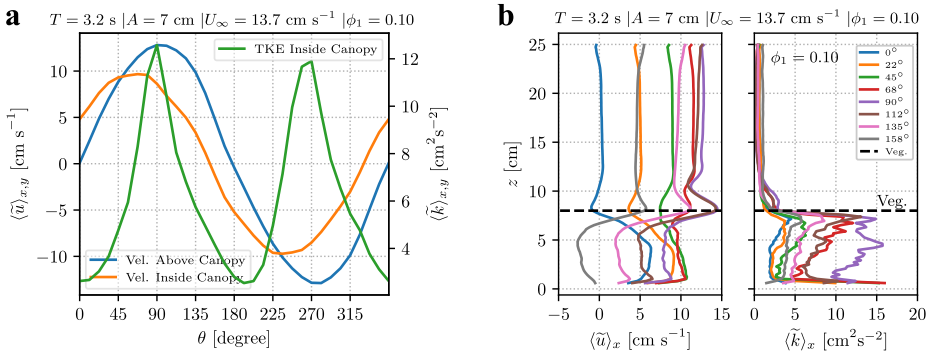

Figure 3. (a) Time series of depth-averaged longitudinal velocity $\widetilde{u}$ above canopy, inside the canopy, and depth-averaged TKE $\widetilde{k}$ inside the canopy for $T = 3.2$ s, $A = 7$ cm, and $\phi_1 = 0.10$. Above the canopy is $z/h > 1$, and inside the canopy $z/h \leq 1$, with z being the vertical coordinate and h vegetation height. (b) Vertical profiles of phase-averaged longitudinal velocity $\widetilde{u}$ and TKE $\widetilde{k}$ over the half positive-velocity cycle for $T = 3.2$ s, $A = 7$ cm, and $\phi_1 = 0.10$.

Flow above the canopy lags behind the flow inside the canopy, while longitudinal velocity is higher above the canopy than inside. For example, one can see the progression between 0° and 90° in any flow-vegetation combination in fig 2. We observe non-zero positive velocity inside the canopy at the beginning of the acceleration phase. Above canopy flow almost catches up with the inside canopy flow at 45° showing timing variations as a function of vegetation density. When the above canopy flow reaches its maximum longitudinal velocity at 90°, the inside flow velocity has already entered into de-

celeration. Notice for instance the difference in velocity change between the profiles 90° and 135° inside and above the canopy.

Turbulent kinetic energy is higher inside the canopy than above the vegetation, with the maximum TKE values at 90°. However, we notice that inside-canopy flow is already decelerating when TKE is at its highest (see fig. 2 and 3a). Figure 3a shows the synchronization between depth-averaged inside canopy and above-canopy velocity with the inside canopy TKE. We observe that the highest TKE values also lag behind the maximum values of longitudinal velocity inside the canopy. The inside canopy flow leads ahead of the above canopy velocity and inside TKE by approximately 22.5°. Figure 3b presents a close-up of longitudinal velocity and TKE profiles for case [$T = 3.2$ s, $A = 7$ cm, and $\phi_1 = 0.10$] at shorter phase-intervals. This TKE profile sequence shows the development of the TKE inside the canopy over half a cycle. It shows that inside-canopy TKE increases as the flow accelerates from 0° to 68°, with the highest values near the top of the canopy and near the bed. However, when the flow reaches 90° (beginning of deceleration phases), TKE becomes more uniform inside the canopy.

3.2 Flow Structure

Between $\phi_4 = 0.04$ and $\phi_3 = 0.05$ there is a vegetation density threshold where canopy-scale structures at the top of the canopy intensify, while stem-wake turbulence decreases. Figure 4 shows normalized vertical profiles of longitudinal and vertical velocities ($\widetilde{u}^*$ and $\widetilde{w}^*$, respectively), turbulent kinetic energy $\widetilde{k}^*$, and Reynolds stress $-\widetilde{u'w'}^*$ for all values of ϕ. We normalize velocity by the maximum outer velocity U_∞ and vertical location by vegetation height h. Figure 4 shows the variation due to wave period and wave amplitude for $\theta = 90°$. Vegetation density $\phi_4 = 0.04$ shows high values of TKE likely generated by wakes inside the canopy, since turbulence is fairly uniform vertically. At vegetation density $\phi_3 = 0.05$, we can observe lower values of TKE inside the canopy but a TKE peak at the top of the canopy. Notice that this peak increases with vegetation density, a sign of stronger shear-induced turbulence at the top of the canopy. We can associate this TKE peaks to an increase in vortex shedding being able to deform the phase-averaged vertical and longitudinal profiles. Take for instance the vertical profiles of $T = 3.2$ s with $A = 10$ cm, and $T = 5.3$ s with $A = 10$ cm. The vertical-velocity component $\widetilde{w}$ shows opposite positive/negative values above and below the top of the canopy, respectively, and is accompanied by a longitudinal velocity $\widetilde{u}$ overshoot at the top of the vegetation. This flow structure suggests the presence of overturn fluid at the top of the canopy that strengthens with vegetation density. These structures are associated with the vegetation density-dependent peaks of TKE and Reynolds stress $\widetilde{u'w'}$ observed at the top of the canopy.

Turbulence intensity at the canopy-top is associated with the excursion length (wave amplitude), while turbulence in the near-bed region results from the contributions of the stem-wake turbulence and shear at the bed (e.g., Tseng & Tinoco, 2021). Vortex shedding at the top of the canopy is more dependent on wave amplitude than on wave period. Compare, for instance, the top and bottom subplot pairs in fig. 4 ($T = 3.2$ s with $A = 10$ cm, and $T = 5.3$ s with $A = 10$ cm, which share a constant wave amplitude) against the top and middle subplot pairs ($T = 3.2$ s with $A = 10$ cm] and [$T = 3.2$ s and $A = 5$ cm], constant wave period). Larger excursion length allows the development of instabilities at the top of the canopy by shear, and hence increases the TKE at the top of the canopy (Ghisalberti & Schlosser, 2013; Y. Zhang et al., 2018; Wong et al., 2019).

It could be argued that near-bed TKE and Reynolds stresses are dominated by stem-wake TKE generation at $\phi_4 = 0.04$. However, for $\phi_3 = 0.05$ or higher, it shifts to a more bed-shear dominated process, since the overall wake turbulence inside the canopy decreases, while TKE and Reynolds stresses increase near the bed (for example, see top row, $T = 3.2$ s with $A = 10$ cm, and bottom row, $T = 5.3$ s with $A = 10$ cm of fig. 4).

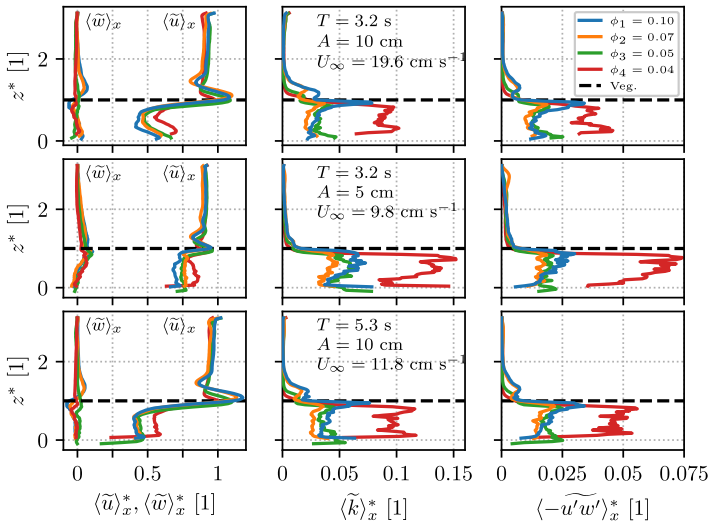

Figure 4. Normalized phase-averaged longitudinal velocity $\widetilde{u}^*$ and vertical velocity $\widetilde{w}^*$ along with phase-averaged TKE $\widetilde{k}^*$ and Reynolds stress $\widetilde{u'w'}^*$ at phase $\theta = 90^\circ$. Velocity is normalized by the maximum outer flow velocity U_∞ and elevation z is normalized by vegetation height h.

Vegetation effects in the form of drag are able to reduce the inside canopy flow enough for the stem-wake turbulence to decrease. Near-bed turbulence is fundamental to sediment transport in oscillatory flows (Garcia, 2008; Tinoco & Coco, 2018). However, the study of individual processes (stem-wake and bed shear) that contribute to the turbulence statistics is hard to separate since they are non-linearly associated (e.g., Tseng & Tinoco, 2021).

3.3 Quadrant analysis

The frequency and intensity of sweep and ejection events at the top of the canopy and near the bed increase with vegetation density. The turbulent event distribution by quadrants Qn ($n = 1, 2, 3, 4$) in fig. 5 indicates the transition between canopy-turbulence to stem-turbulence across the mixing layer at the top of the canopy and stem- to bed-shear turbulence near the bed. Figure 5 shows the proportion of turbulent events in a $u'-w'$ space at four regions (illustrated later in fig. 8a) in a vegetated oscillatory flow: outer flow (above the canopy, $1.9 < z/h < 2.5$), mixing layer at the top of the canopy ($1 - \Delta_{\mathrm{mix}}/2h < z/h < 1 + \Delta_{\mathrm{mix}}/2h$, see section 4.2 for mixing layer width Δ_{mix}), inside the canopy in the stem-wake region ($0.4 < z/h < 0.6$), and near the bed ($z/h < z_{\mathrm{bedform}}/h + 0.05$, where z_{bedform} is the elevation of the bedforms in the mobile bed). Here, we define ejections as the quadrant 2-events (Q2), and sweeps as the quadrant 4-events (Q4) in the $u'-w'$ sample space (Pope, 2001). In the outer flow, where no vegetation is present, the flow is dominated by ejections. In the presence of vegetation, ejections begin to compete with sweeps. In the mixing layer, we observe that the flow moves from sweeps- to sweeps-and-ejection-dominated flows with increasing vegetation density. We also notice that inside the canopy there is a more even distribution of turbulent events across the quadrant. This indicates that flow may be dominated by lateral fluctuations due to being a wake dominated zone. Finally, near the bed the turbulent events are dominated again by sweeps and ejections with relatively high contributions from other quadrants, which shows a significant contribution of the near-bed boundary layer flow inside a stem-wake dominated region.

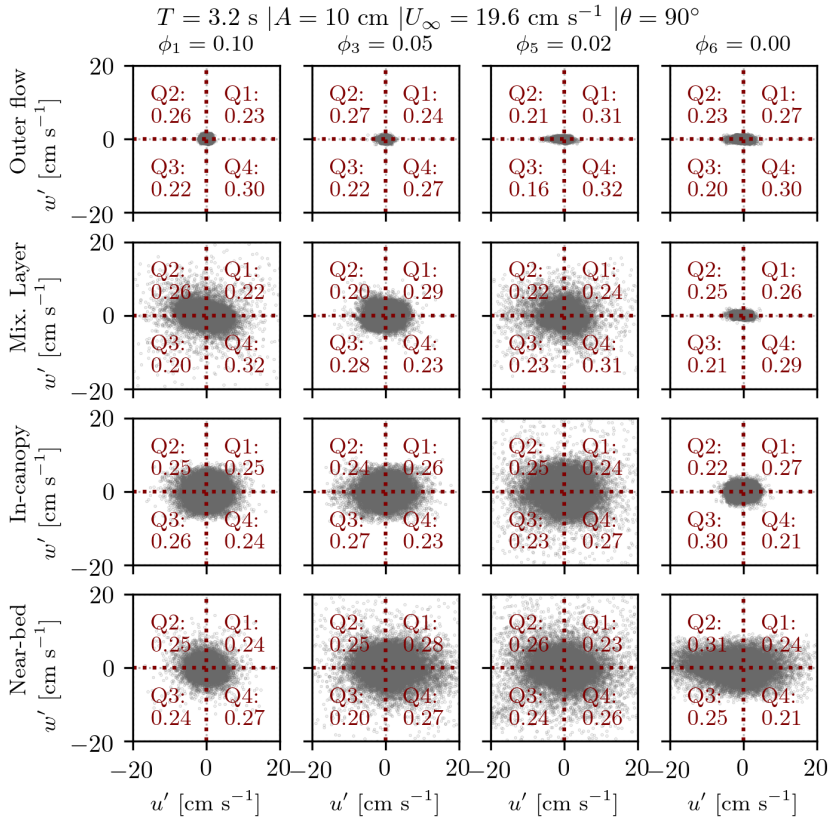

Figure 5. Distribution of turbulent events in a $u' - w'$ sample space for flow condition $T = 3.2$ s and $A = 10$ cm at $\theta = 90°$. Each subplot presents the proportion of events per quadrant. Vertically we present different zones in a vegetated flow and horizontally we show four vegetation conditions, $\phi_1 = 0.10$ to $\phi_1 = 0$ (no-vegetation).

4 Turbulent Kinetic Energy Predictors

4.1 Maximum Turbulent Kinetic Energy Near the Bed

We present a relation to estimate the maximum turbulent kinetic energy (TKE) near the bed using the maximum depth-averaged longitudinal velocity inside the canopy U_{in} and volumetric solid fraction ϕ of the canopy. It becomes a convenient tool to assess the potential of sediment routing due to TKE inside a vegetation patch in wave-dominated environments (e.g. Tinoco & Coco, 2018). Thus, it may improve simplified transport models for restoration and morphodynamic evolution of coastal and estuarine ecosystems.

Our formulation follows the model structure proposed by Tanino and Nepf (2008b, eq. 4.1). Their model originally was developed for emergent, unidirectional, vegetated flows where the TKE budget reduces to a balance between stem-wake turbulence production and TKE viscous dissipation (e.g. Raupach & Shaw, 1982; Burke & Stolzenbach, 1983). Tanino and Nepf (2008b)'s model has been modified and used in oscillatory flows to estimate averaged-turbulence intensities through vegetation (e.g. Y. Zhang et al., 2018; Chen et al., 2020). However, these adapted models do not capture the peak of turbulence intensities near the bed over a wave cycle. As a function of bed roughness, wake-contributions, and bedform-induced turbulence, bursts of high turbulence intensity are the most important mechanism for potential entrainment and resuspension of sediment in oscillatory flows (Yang & Nepf, 2018; Y. Zhang & Nepf, 2019). Equation 10 follows the same form of Tanino and Nepf (2008b)'s model, where k is TKE, U_p is cross-section averaged flow velocity, C_D is drag coefficient, d is stem diameter, and $\langle s_n \rangle_A$ is the average stem spacing.

$$\left\langle \frac{\sqrt{k}}{U_p} \right\rangle = \begin{cases} 1.1 \left[C_D \dfrac{\phi}{(1-\phi)\pi/2} \right]^{1/3} & d/\langle s_n \rangle_A < 0.56 \\ 0.88 \left[C_D \dfrac{\langle s_n \rangle_A}{d} \dfrac{\phi}{(1-\phi)\pi/2} \right]^{1/3} & d/\langle s_n \rangle_A \geq 0.56 \end{cases} \tag{10}$$

We propose a relation for the maximum near-bed TKE since this variable is the main driver of sediment resuspension in oscillatory flows (Tinoco & Coco, 2018). Equation 11 presents a modified form of Tanino and Nepf (2008b)'s model for $d/\langle s_n \rangle_A < 0.56$ (within which our experimental cases fall). Where $k_{\text{bed}}^{1/2}$ is the maximum phase-averaged near-bed TKE over a wave cycle. Drag coefficient C_D is set to be a function of wave parameters (A and T) and stem diameter d, and the proportional constant δ_ϕ becomes a function of ϕ. We adjust linear regressions to series of maximum near-bed TKE and inside-canopy velocity for several vegetation densities and present them in figure 6.

$$\frac{k_{\text{bed}}^{1/2}}{U_{\text{in}}} = \delta_\phi(\phi) \left[C_D(A,T,d) \frac{\phi}{(1-\phi)\pi/2} \right]^{1/3} \qquad d/\langle s_n \rangle_A < 0.56 \tag{11}$$

According to the linear regressions presented in fig. 6, δ_ϕ varies between 0.81 and 1.27 as a function of vegetation density. The variation of δ_ϕ coefficient as a function of ϕ may be attributed to inaccurate estimations of drag coefficient. Lacking a better model to estimate C_D for oscillatory flow, Ghisalberti and Schlosser (2013, eq. 9) propose the use of equation 12 (White and Corfield (2006), $\text{Re}_{\text{eq}} = [2\pi A/T]d/\nu$) for sparse enough vegetation and weak dependence to KC. Studies on vegetation drag coincide that drag coefficient depends on vegetation density ϕ (e.g., Tanino & Nepf, 2008a; Tinoco & Cowen, 2013). However, its behavior still remains a subject for further research given the unsteady and reversal nature of wave-dominated flows.

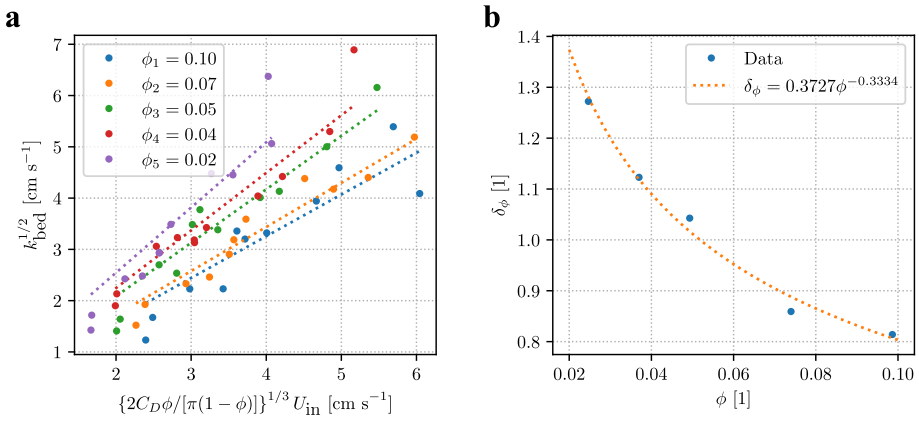

Figure 6. (a) Maximum turbulent kinetic energy as a function of vegetation density and maximum depth-averaged velocity inside the canopy. (b) Empirical regression between values of $\delta_\phi(\phi)$ and ϕ.

$$C_D = 1.0 + 10.0\mathrm{Re}_{\mathrm{eq}}^{-2/3} \tag{12}$$

We fit an empirical power-law regression to the values of $\delta_\phi(\phi)$ extracted from figure 6a as a function of ϕ (see figure 6b). From the empirical regression we found $\delta_\phi(\phi) = 0.37\phi^{-0.33}$. Attributing this vegetation-dependence variation to the drag coefficient, we modify the drag coefficient formulation into equation 13. Where C_D was estimated using equation 12 for the sparsest vegetation case $\phi_5 = 0.02$ as a reference.

$$C_{D,\phi} = \left[1 + 10\mathrm{Re}_{\mathrm{eq}}^{-2/3}\right](0.37\phi^{-0.33}) \tag{13}$$

This modification produces drag coefficient within expected values (0.92 to 1.64). It still could be argued that the total TKE produced near the bed is highly influenced by additional mechanisms, such as bed shear and bedform contributions. Authors have proposed a function for near-bed TKE that results from the summation of a bed-shear contribution and stem-wake where their mutual influence is neglected (e.g., Yang et al., 2016; Tinoco & Coco, 2018). This approach becomes appropriate to establish a reference condition (bare bed) to study the onset of incipient motion in vegetated flows. Yet, it cannot be extended to near-bed TKE estimations because of the reciprocal interaction between TKE and bed dynamics. Due to the difficulty to separate each individual contribution near the bed, they are compound within the vegetation-dependence variation of the coefficient $\delta_\phi(\phi)$ and $C_D(\mathrm{Re}_{\mathrm{eq}})$. In contrast to Yang et al. (2016)'s work in unidirectional currents with emergent vegetation, our results show a stronger dependence between vegetation density and turbulence production near the bed for oscillatory flows. Incorporating $\delta_\phi(\phi)$ relation into equation 11 for maximum near-bed TKE, we obtain equation 14. Figure 7a presents our model along with the experimental data.

$$\frac{k_{\mathrm{bed}}^{1/2}}{U_{\mathrm{in}}} = 0.37\left[C_D(\mathrm{Re}_{\mathrm{eq}})\frac{\phi}{(1-\phi)\pi/2}\right]^{1/3}\phi^{-0.33} \qquad d/\langle s_n\rangle_A < 0.56 \tag{14}$$

Figure 7b contrasts our experimental results and model, against Tanino and Nepf (2008b)'s available data and model. They measure instantaneous flow velocity from $z = 0.17H$ up to $z = 0.85H$ (H flow depth). Turbulence intensity in emergent vegetated

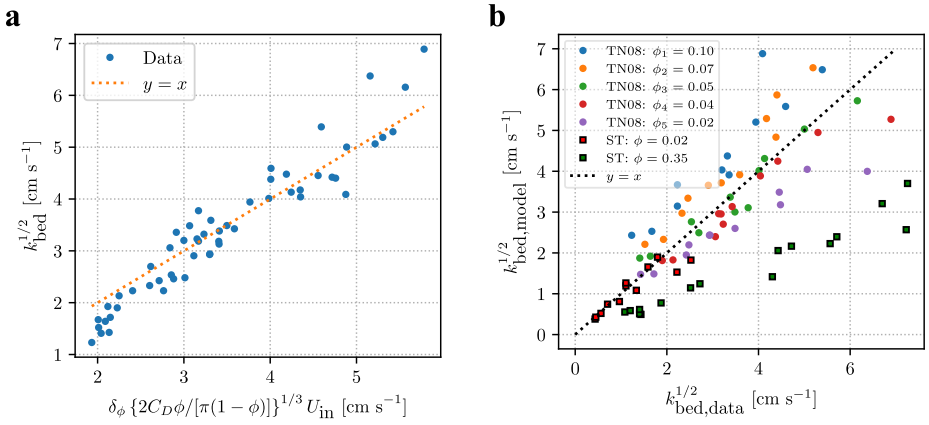

Figure 7. (a) Predicted maximum turbulent kinetic energy near the bed as a function of vegetation density and maximum depth-averaged velocity inside the canopy. (b) Comparison between Tanino and Nepf (2008)'s model (TN08) and their available data with our proposed model (ST) and experimental data

flows is the highest near the bed and decreases towards the water surface. Therefore, we selected the maximum values of TKE from the series presented in Tanino and Nepf (2008b) for comparison. Our model predicts Tanino and Nepf (2008b)'s available data (maximum TKE) well for $\phi = 0.02$. Even though their flow is unidirectional, our predictor has a good agreement with their data. In the case of $\phi = 0.35$, our predictions underestimate their data. This vegetation density is higher than the densities used in our study (approximately three times our densest case). It indicates that our predictor may not be applicable to denser canopy flows.

Tanino and Nepf (2008b) model's prediction of our experimental data follows the main trend of the data. However, their model underestimates values of TKE for cases of $\phi_5 = 0.02$ while it overestimate for $\phi_2 = 0.07$ and $\phi_1 = 0.10$. Their predictor was developed for emergent-canopy unidirectional flows, far from the effect of the bed. Therefore, sediment roughness and bedforms hinder the applicability of this models to our experimental results.

4.2 Maximum Turbulent Kinetic Energy Across the Top of the Canopy

We propose two relations to predict the maximum TKE at the top of the canopy k_{top}, set by the vegetation density threshold found on section 3. The first predictor estimates the phase-averaged variation of k_{top} when the turbulence inside the canopy is dominated by stem-wakes and there is a weak contribution from the canopy-scale turbulence at top of the canopy. The second predictor estimates k_{top} for a regime where vegetation drag reduces flow velocity inside the canopy hindering stem-wake turbulence, but the transfer of TKE from canopy-scale eddies into stem-wake inside the mixing layer strengthens. Each expression is set as a function of the outer flow above the canopy (to allow for predictions with easy-to-measure velocities) and vegetation density.

We define the TKE at the top of the canopy as the spatial averaged TKE within the width of the mixing layer Δ_{mix} (see figure 8a), where Δ_{mix} is characterized by the vorticity thickness $\Delta U/(\partial\widetilde{u}/\partial z)$ and ΔU is the absolute difference between the depth-averaged velocity inside and above the canopy (Finnigan, 2000). Turbulence dynamics within the mixing layer thickness experience a rapid energy transfer where canopy-scale eddies lose their TKE directly into wake TKE in a so-called spectral short-cut (Finnigan,

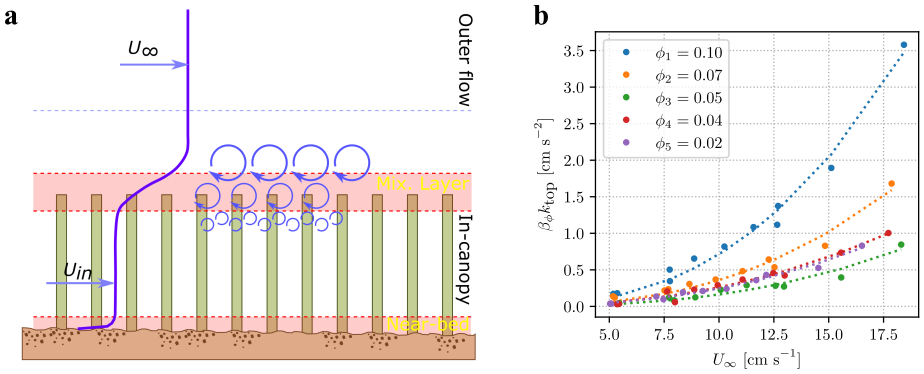

Figure 8. (a) Illustration of Turbulent Kinetic Energy at the top of the canopy k_{top} within the mixing layer Δ_{mix} and outer velocity U_∞. (b) Scatter plot of the variation of βk_{top} as a function of outer flow velocity U_∞ grouped by volumetric solid fraction ϕ.

Table 2. Fitting coefficients α_ϕ and power ψ from power-function regression for maximum canopy-top TKE with their respective R^2 coefficient.

ϕ	α_ϕ	ψ	R^2
0.10	0.0018	2.59	0.99
0.07	0.0010	2.56	0.97
0.05	0.0004	2.59	0.94
0.04	0.0012	2.34	0.98
0.02	0.0011	2.36	0.98

2000; King et al., 2012). The rate of TKE transfer in this region is proportional to the work done by these eddies against the vegetation drag.

To incorporate the effect of vegetation, we employ the rate of work done by the canopy-scale eddies against the vegetation drag as the transfer mechanism for TKE into wake turbulence inside the mixing layer. Finnigan (2000, eq. 6.7) and King et al. (2012, eq. 3.12) propose equation 15 to express the rate of work done by the velocity fluctuations in the mixing layer, where C_D is the drag coefficient, a is the volumetric frontal area, ϕ is volumetric solid fraction, $|U|$ is mean characteristic velocity, and $1/2\langle\overline{u_i' u_i'}\rangle$ is the TKE within the mixing layer, k_{top}.

$$W \approx \frac{3}{4}\frac{C_D a}{1-\phi}|U|\frac{1}{2}\langle\overline{u_i' u_i'}\rangle \tag{15}$$

Figure 8b presents the variation of $\beta_\phi k_{\text{top}}$ as a function of U_∞, where $\beta_\phi = C_D a/(1-\phi)$ for each vegetation density ($\phi_1 = 0.10$ to $\phi_5 = 0.02$). Each vegetation data set follows a power function tendency of the form seen in equation 16, where α_ϕ and ψ are coefficients that depend on vegetation density, as listed in Table 2.

$$\beta_\phi k_{\text{top}} = \alpha_\phi U_\infty^\psi \tag{16}$$

Data from vegetation density $\phi_5 = 0.02$ and $\phi_4 = 0.04$ collapse into the same curve. This is because turbulence under these vegetation conditions are dominated by

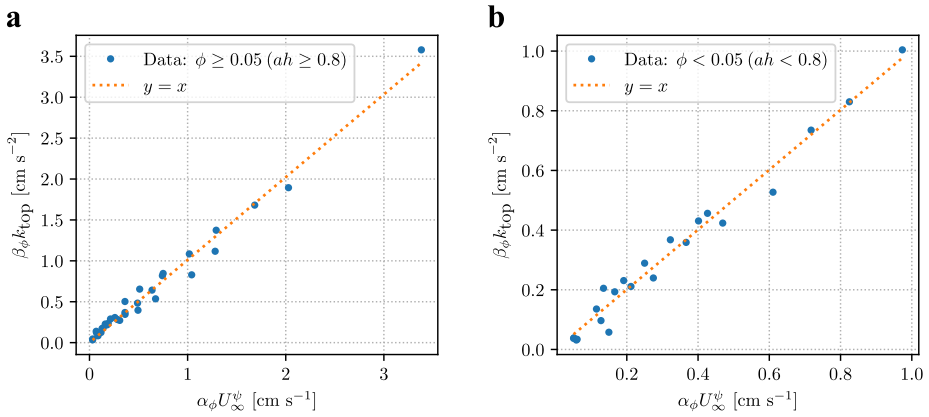

Figure 9. (a) Distribution of βk_{top} as a function of outer flow velocity U_∞ for $\phi \geq 0.05(ah \geq 0.8)$, where $\beta_\phi = C_D a/(1-\phi)$. (b) Distribution of βk_{top} as a function of outer flow velocity U_∞ for $\phi < 0.05(ah < 0.8)$.

stem wakes. Therefore, the energy transfer from shear at the top of the canopy into the stem-wake is weak enough that it becomes invariant of vegetation density. As vegetation density increases to $\phi_3 = 0.05$, values of $\beta_\phi k_{\text{top}}$ decrease compared to the sparser cases. This behavior marks a transition where aquatic vegetation hinders the turbulence transfer from the mixing layer into the canopy. From this vegetation condition on to denser cases, values of $\beta_\phi k_{\text{top}}$ increase with ϕ, with canopy-scale eddies growing strong enough to interact with the vegetation drag at the top of the canopy increasing the rate of kinetic energy transfer. Table 2 shows that $\beta_\phi k_{top}$ over vegetation density from $\phi_3 = 0.05$ to $\phi_1 = 0.10$ increases to the power of 2.58. On the other hand, for vegetation density $\phi_5 = 0.02$ to $\phi_4 = 0.04$, $\beta_\phi k_{top}$ increases as a function of outer velocity following a power function to 2.35 power. We thus propose a two-regime empirical predictor for TKE levels at the top of the canopy as a function of outer flow velocity and vegetation density (see eq. 17, as shown in fig. 9a and 9b). Data in figs 9a and 9b also provide a benchmark for numerical models on the rate of work done by the eddies against the vegetation drag inside the mixing layer thickness.

$$\beta_\phi k_{\text{top}} = \begin{cases} 0.0011 U_\infty^{2.35} & \phi < 0.05 \quad (ah < 0.8) \\ \\ 0.26 \phi^{2.15} U_\infty^{2.58} & \phi \geq 0.05 \quad (ah \geq 0.8) \end{cases} \tag{17}$$

5 Conclusions

We studied flow and turbulence structure in oscillatory flows through submerged vegetation associated with the turbulent kinetic energy generated at the top of the canopy and near the bed. We used particle image velocimetry to measure velocity fields inside and above the vegetation. We analyzed the temporal and spatial evolution of velocity and turbulent profiles, such as Reynolds stresses and turbulent events (quadrant analysis). We developed two empirical relations for maximum TKE at the top of the canopy mixing layer and near the bed. We found that vegetation density and wave amplitude (excursion length) determine the structure and timing of vegetated oscillatory flows.

We noticed that maximum values of TKE inside the canopy follow a non-monotonic relation with vegetation density. We found that for $\phi < 0.05$ ($ah < 0.8$) turbulence inside the canopy is dominated by stem-wake turbulence. However, stem-scale turbu-

lence decreases while canopy-scale turbulence at the top of the canopy strengthens for $\phi \geq 0.05$ ($ah \geq 0.8$). Quadrant analysis also shows that the frequency and intensity of sweep and ejection events at the top of the canopy and near the bed increases with the vegetation density in the latter regime.

We propose two relations to predict the maximum TKE at the top of the canopy (inside the mixing layer) as a function of the vegetation density and maximum outer velocity. To quantify the effect of vegetation density, we used the rate of work done by the canopy-scale eddies against the vegetation drag as the transfer mechanism for the TKE into wake turbulence inside the mixing layer. In stem-wake dominated flow, $\beta_\phi k_{\text{top}}$ is invariant to vegetation density for $\phi < 0.05$ ($ah < 0.8$) following a power function with respect to outer velocity. On the other hand, $\beta_\phi k_{\text{top}}$ increases as a function of vegetation density for $\phi \geq 0.05$ ($ah \geq 0.8$) where canopy-scale turbulence strengthens by shear at the top of the canopy following another power function.

We also present a relation to estimate the maximum TKE near the bed using the maximum depth-averaged longitudinal velocity inside the canopy and volumetric solid fraction of the canopy. Our formulation follows the model structure proposed by Tanino and Nepf (2008b), but adjusted to consider maximum values of TKE under oscillatory conditions instead of time averages. According to our linear regressions, δ_ϕ varies between 0.81 and 1.27 as a function of vegetation density, yielding an empirical regression of $\delta_\phi = 0.37\phi^{-0.33}$.

The set of TKE models presented here provide easy-to-use tools for the estimation of maximum turbulence intensities at the canopy top and near the bed. Both predictors require vegetation density information in the form of volumetric solid fraction ϕ and maximum outer flow velocity U_∞. They become practical formulations for environmental engineering applications, as maximum TKE at the top of the canopy controls mass exchange and mixing across the vegetation top, whereas maximum TKE near the bed becomes a key mechanism for sediment transport in vegetated oscillatory flows.

Acknowledgments

JES acknowledges funding support from UIUC-CEE Departmental Funds. This study was supported by NSF through CAREER EAR 1753200. Any opinions, findings and conclusions or recommendations expressed in this material are those of the authors and do not necessarily reflect those of the National Science Foundation. The datasets generated during and/or analyzed are available in the Figshare repository, (DOI provided after acceptance).

References

Abdolahpour, M., Ghisalberti, M., McMahon, K., & Lavery, P. S. (2018). The impact of flexibility on flow, turbulence, and vertical mixing in coastal canopies. *Limnology and Oceanography*, *63*(6), 2777–2792.

Bouma, T., Van Duren, L., Temmerman, S., Claverie, T., Blanco-Garcia, A., Ysebaert, T., & Herman, P. (2007). Spatial flow and sedimentation patterns within patches of epibenthic structures: Combining field, flume and modelling experiments. *Continental Shelf Research*, *27*(8), 1020–1045.

Burke, R. W., & Stolzenbach, K. D. (1983, June). *Free surface flow through salt marsh grass* (MITSG No. 83-16). MIT.

Chen, M., Lou, S., Liu, S., Ma, G., Liu, H., Zhong, G., & Zhang, H. (2020). Velocity and turbulence affected by submerged rigid vegetation under waves, currents and combined wave–current flows. *Coastal Engineering*, 103727.

Davis, K. A., Pawlak, G., & Monismith, S. G. (2020). Turbulence and coral reefs. *Annual Review of Marine Science*, *13*.

Finnigan, J. (2000). Turbulence in plant canopies. *Annual review of fluid mechanics*, *32*(1), 519–571.

Garcia, M. (2008). Sedimentation engineering: processes, measurements, modeling, and practice..

Ghisalberti, M., & Nepf, H. M. (2002). Mixing layers and coherent structures in vegetated aquatic flows. *Journal of Geophysical Research: Oceans*, *107*(C2), 3–1.

Ghisalberti, M., & Schlosser, T. (2013). Vortex generation in oscillatory canopy flow. *Journal of Geophysical Research: Oceans*, *118*(3), 1534–1542.

Hansen, J. C., & Reidenbach, M. A. (2017). Turbulent mixing and fluid transport within florida bay seagrass meadows. *Advances in Water Resources*, *108*, 205 - 215.

Jensen, B., Sumer, B., & Fredsøe, J. (1989). Turbulent oscillatory boundary layers at high reynolds numbers. *Journal of Fluid Mechanics*, *206*, 265–297.

King, A. T., Tinoco, R. O., & Cowen, E. A. (2012). A k-[epsilon] turbulence model based on the scales of vertical shear and stem wakes valid for emergent and submerged vegetated flows. *Journal of Fluid Mechanics*, *701*, 1.

Leonard, L. A., & Luther, M. E. (1995). Flow hydrodynamics in tidal marsh canopies. *Limnology and oceanography*, *40*(8), 1474–1484.

López, F., & García, M. H. (2001). Mean flow and turbulence structure of open-channel flow through non-emergent vegetation. *Journal of Hydraulic Engineering*, *127*(5), 392–402.

Lowe, R. J., Koseff, J. R., & Monismith, S. G. (2005). Oscillatory flow through submerged canopies: 1. velocity structure. *Journal of Geophysical Research: Oceans*, *110*(C10).

Lowe, R. J., Koseff, J. R., Monismith, S. G., & Falter, J. L. (2005). Oscillatory flow through submerged canopies: 2. canopy mass transfer. *Journal of Geophysical Research: Oceans*, *110*(C10).

Nepf, H. M. (2012). Hydrodynamics of vegetated channels. *Journal of Hydraulic Research*, *50*(3), 262–279.

Norris, B. K., Mullarney, J. C., Bryan, K. R., & Henderson, S. M. (2017). The effect of pneumatophore density on turbulence: A field study in a sonneratia-dominated mangrove forest, vietnam. *Continental Shelf Research*, *147*, 114–127.

Norris, B. K., Mullarney, J. C., Bryan, K. R., & Henderson, S. M. (2019). Turbulence within natural mangrove pneumatophore canopies. *Journal of Geophysical Research: Oceans*, *124*(4), 2263-2288.

Perillo, G., & Piccolo, M. (2011). Global variability in estuaries and coastal settings. In E. Wolanski & D. McLusky (Eds.), *Treatise on estuarine and coastal science* (Vol. 1, pp. 7–36). Waltham: Academic Press.

Pope, S. B. (2001). *Turbulent flows*. IOP Publishing.

Pujol, D., Casamitjana, X., Serra, T., & Colomer, J. (2013). Canopy-scale turbulence under oscillatory flow. *Continental Shelf Research*, *66*, 9–18.

Pujol, D., Serra, T., Colomer, J., & Casamitjana, X. (2013). Flow structure in canopy models dominated by progressive waves. *Journal of hydrology*, *486*, 281–292.

Raupach, M. R., & Shaw, R. (1982). Averaging procedures for flow within vegetation canopies. *Boundary-Layer Meteorology*, *22*(1), 79–90.

Shan, Y., Zhao, T., Liu, C., & Nepf, H. (2020). Turbulence and bed-load transport in channels with randomly distributed emergent patches of model vegetation. *Geophysical Research Letters*, e2020GL087055.

Tang, C., Lei, J., & Nepf, H. M. (2019). Impact of vegetation-generated turbulence on the critical, near-bed, wave-velocity for sediment resuspension. *Water Resources Research*, *55*(7), 5904–5917.

Tanino, Y., & Nepf, H. M. (2008a). Laboratory investigation of mean drag in a random array of rigid, emergent cylinders. *Journal of Hydraulic Engineering*,

134(1), 34–41.

Tanino, Y., & Nepf, H. M. (2008b). Lateral dispersion in random cylinder arrays at high reynolds number. *Journal of Fluid Mechanics*, *600*, 339–371.

Thielicke, W., & Stamhuis, E. (2014). Pivlab–towards user-friendly, affordable and accurate digital particle image velocimetry in matlab. *Journal of open research software*, *2*(1).

Tinoco, R. O., & Coco, G. (2018). Turbulence as the main driver of resuspension in oscillatory flow through vegetation. *Journal of Geophysical Research: Earth Surface*, *123*(5), 891–904.

Tinoco, R. O., & Cowen, E. A. (2013). The direct and indirect measurement of boundary stress and drag on individual and complex arrays of elements. *Experiments in fluids*, *54*(4), 1509.

Tseng, C.-Y., & Tinoco, R. O. (2021). A two-layer turbulence-based model to predict suspended sediment concentration in flows with aquatic vegetation. *Geophysical Research Letters*, *48*, e2020GL091255.

White, F. M., & Corfield, I. (2006). *Viscous fluid flow* (Vol. 3). McGraw-Hill New York.

Wong, C. Y., Trinh, P. H., & Chapman, S. J. (2019). Shear-induced instabilities of flows through submerged vegetation. *arXiv preprint arXiv:1904.11981*.

Yang, J., Chung, H., & Nepf, H. (2016). The onset of sediment transport in vegetated channels predicted by turbulent kinetic energy. *Geophysical Research Letters*, *43*(21), 11–261.

Yang, J., & Nepf, H. (2018). A turbulence-based bed-load transport model for bare and vegetated channels. *Geophysical Research Letters*, *45*(19), 10–428.

Zhang, J., Lei, J., Huai, W., & Nepf, H. (2020). Turbulence and particle deposition under steady flow along a submerged seagrass meadow. *Journal of Geophysical Research: Oceans*, *125*(5), e2019JC015985.

Zhang, Y., & Nepf, H. (2019). Wave-driven sediment resuspension within a model eelgrass meadow. *Journal of Geophysical Research: Earth Surface*, *124*(4), 1035–1053.

Zhang, Y., Tang, C., & Nepf, H. (2018). Turbulent kinetic energy in submerged model canopies under oscillatory flow. *Water Resources Research*, *54*(3), 1734–1750.

Zhao, H., Tang, H., Yan, J., Liang, D., & Zheng, J. (2020). Spectral shortcut in turbulence energy transfer in open channel flow over submerged vegetation. *Journal of Hydro-environment Research*, *33*, 10–18.